IMAGING OF A TRANSITIONAL DISK GAP IN REFLECTED LIGHT: INDICATIONS OF PLANET FORMATION AROUND THE YOUNG SOLAR ANALOG LkCa 15[*]

C. Thalmann[1], C. A. Grady[2], M. Goto[1], J. P. Wisniewski[3], M. Janson[4], T. Henning[1], M. Fukagawa[5], M. Honda[6], G. D. Mulders[7,8], M. Min[9], A. Moro-Martín[10,11], M. W. McElwain[11], K. W. Hodapp[12], J. Carson[1,13], L. Abe[14], W. Brandner[1], S. Egner[15], M. Feldt[1], T. Fukue[16], T. Golota[15], O. Guyon[15], J. Hashimoto[16], Y. Hayano[15], M. Hayashi[15], S. Hayashi[15], M. Ishii[15], R. Kandori[16], G. R. Knapp[11], T. Kudo[16], N. Kusakabe[16], M. Kuzuhara[16,17], T. Matsuo[16], S. Miyama[16], J.-I. Morino[16], T. Nishimura[15], T.-S. Pyo[15], E. Serabyn[18], H. Shibai[5], H. Suto[16], R. Suzuki[16], M. Takami[19], N. Takato[15], H. Terada[15], D. Tomono[15], E. L. Turner[11,20], M. Watanabe[21], T. Yamada[22], H. Takami[15], T. Usuda[15], and M. Tamura[16]

[1] Max Planck Institute for Astronomy, Heidelberg, Germany; thalmann@mpia.de
[2] Eureka Scientific and Goddard Space Flight Center, Greenbelt, USA
[3] University of Washington, Seattle, Washington, USA
[4] University of Toronto, Toronto, Canada
[5] Osaka University, Osaka, Japan
[6] Faculty of Science, Kanagawa University, Kanagawa, Japan
[7] Astronomical Institute "Anton Pannekoek," University of Amsterdam, Amsterdam, The Netherlands
[8] SRON Netherlands Institute for Space Research, Groningen, The Netherlands
[9] Astronomical Institute, University of Utrecht, Utrecht, The Netherlands
[10] Department of Astrophysics, CAB-CSIC/INTA, Madrid, Spain
[11] Department of Astrophysical Sciences, Princeton University, Princeton, USA
[12] Institute for Astronomy, University of Hawai'i, Hilo, Hawai'i, USA
[13] College of Charleston, Charleston, South Carolina, USA
[14] Laboratoire Hippolyte Fizeau, Nice, France
[15] Subaru Telescope, Hilo, Hawai'i, USA
[16] National Astronomical Observatory of Japan, Tokyo, Japan
[17] University of Tokyo, Tokyo, Japan
[18] JPL, California Institute of Technology, Pasadena, USA
[19] Institute of Astronomy and Astrophysics, Academia Sinica, Taipei, Taiwan
[20] Institute for the Physics and Mathematics of the Universe, University of Tokyo, Japan
[21] Department of Cosmosciences, Hokkaido University, Sapporo, Japan
[22] Astronomical Institute, Tohoku University, Sendai, Japan

ABSTRACT

We present H- and K_s-band imaging data resolving the gap in the transitional disk around LkCa 15, revealing the surrounding nebulosity. We detect sharp elliptical contours delimiting the nebulosity on the inside as well as the outside, consistent with the shape, size, ellipticity, and orientation of starlight reflected from the far-side disk wall, whereas the near-side wall is shielded from view by the disk's optically thick bulk. We note that forward scattering of starlight on the near-side disk surface could provide an alternate interpretation of the nebulosity. In either case, this discovery provides confirmation of the disk geometry that has been proposed to explain the spectral energy distributions of such systems, comprising an optically thick disk with an inner truncation radius of ∼46 AU enclosing a largely evacuated gap. Our data show an offset of the nebulosity contours along the major axis, likely corresponding to a physical pericenter offset of the disk gap. This reinforces the leading theory that dynamical clearing by at least one orbiting body is the cause of the gap. Based on evolutionary models, our high-contrast imagery imposes an upper limit of 21 $M_{\rm Jup}$ on companions at separations outside of 0″.1 and of 13 $M_{\rm Jup}$ outside of 0″.2. Thus, we find that a planetary system around LkCa 15 is the most likely explanation for the disk architecture.

Key words: circumstellar matter – planetary systems – stars: individual (LkCa 15) – stars: pre-main sequence – techniques: high angular resolution

Online-only material: color figures

1. INTRODUCTION

The circumstellar disks of gas and dust around newly formed stars are believed to be the birthplaces of giant planets. In some protoplanetary disks, evidence of gaps or inner cavities has been revealed through analysis of the infrared spectral energy distribution (SED; e.g., Calvet et al. 2002) or interferometry at infrared (e.g., Ratzka et al. 2007) or millimeter wavelengths (e.g., Brown et al. 2009). These objects have been termed "transi-

tional disks," since they are thought to represent a transitional state of partial disk dissipation between the protoplanetary disk stage and the debris disk stage, with a variety of mechanisms proposed to account for central cavities: photoevaporation, disk instabilities, and dynamical clearing (Alexander et al. 2006; Chiang & Murray-Clay 2007; Bryden et al. 1999).

One such system is LkCa 15 (K5:Ve, $V = 11.91$ mag, $J = 9.42$ mag, $H = 8.6$ mag, $K = 8.16$ mag), a 0.97 $M_\odot$, 3–5 Myr old (Simon et al. 2000), weak-line T Tauri star with a gas-rich millimeter-bright disk (Piétu et al. 2007; Henning et al. 2010). Recently, it was identified as a pre-transitional disk (Espaillat et al. 2007), which consists of an inner disk component near the dust sublimation radius (0.12–0.15 AU), a wide gap, and

an outer disk beyond 46 AU (Espaillat et al. 2008). *Spitzer* IRS spectra by Sargent et al. (2009) reveal a relatively low level of dust grain growth. With an expected angular scale of 0″33, the outer wall is accessible to 8 m class telescopes equipped with high-contrast imagers.

2. OBSERVATIONS AND DATA REDUCTION

2.1. Subaru/HiCIAO Data

As part of the ongoing high-contrast imaging survey Strategic Exploration of Exoplanets and Disks with Subaru/HiCIAO (SEEDS; Tamura 2009), we observed LkCa 15 on 2009 December 26, with the HiCIAO instrument (Hodapp et al. 2008) on the Subaru Telescope with a field of view of $20'' \times 20''$ and a plate scale of 9.5 mas pixel^{-1}. The images were taken in *H* band (1.6 m), and the image rotator was operated in pupil-tracking mode to enable angular differential imaging (ADI; Marois et al. 2006). The data set comprises 168 frames, each containing the co-add of three unsaturated exposures of 1.39 s, for a total integration time of 700.6 s. The image resolution provided by the adaptive optics system AO188 was close to the diffraction limit, with an FWHM of 55 mas at 0″6 natural seeing in *H*.

The data were corrected for flat field and field distortion. In order to search for point sources such as planets, ADI was then performed on the images using the locally optimized combination of images algorithm (LOCI; Lafrenière et al. 2007). This form of ADI is the most powerful high-contrast imaging method currently available, as evidenced by recent direct detections of substellar companions (Marois et al. 2008; Thalmann et al. 2009).

For two frames to be eligible for mutual point-spread function (PSF) subtraction at a given working radius, we require the differential field rotation arc at that radius to be at least 3 FWHM = 165 mas, as opposed to the 0.75 FWHM typically used for the detection of point sources. This protects extended structures of up to the given azimuthal size scale from self-subtraction. We refer to this technique as "conservative LOCI." A circularly symmetric circumstellar structure is still eliminated under these conditions, but as our data demonstrate, a sufficiently elliptical structure can survive by intersecting the concentric annuli around the star at a steep angle.

An alternate method to reveal circumstellar nebulosity is subtraction of the PSF of a reference star, which avoids disk self-subtraction at the price of less effective stellar PSF removal. We observed the star SAO 76662 in pupil-tracking mode immediately after LkCa 15 for this purpose. A neutral density filter was used with the adaptive optics wave-front sensor to achieve the same PSF quality as with the fainter LkCa 15. The exposures were centered, flat-fielded, distortion-corrected, and directly collapsed with a pixelwise median. We subtracted the resulting reference PSF from each of the LkCa 15 frames before de-rotation and co-addition to ensure optimal matching of the pupil-stabilized stellar PSFs.

2.2. Archival VLT/NACO Data

For comparison, we retrieved K_s-band coronagraphic imaging data of LkCa 15 taken with Very Large Telescope (VLT)/NACO in 2007 from the ESO Science Archive Facility under the program ID 280.C-5033(A). The observations were made in field-tracking mode and thus could not be used for LOCI. However, a reference star is included in the data set, allowing PSF subtraction. The camera with 13 mas pixel scale and the four-quadrant phase mask coronagraph had been used
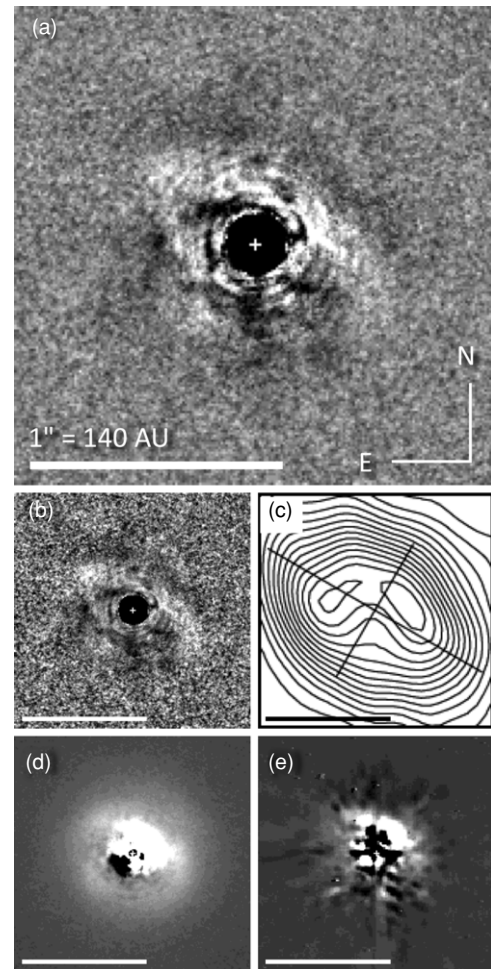

Figure 1. High-contrast imaging of LkCa 15. The scale bars in all panels correspond to $1'' = 140$ AU in projected separation. The gray scale is linear. (a) HiCIAO *H*-band image after conservative LOCI ADI. The inner edge of the outer disk is clearly visible. The blacked-out area in the center represents the range of separations where the field rotation is insufficient for ADI. The negative features within 0″5 are areas oversubtracted by LOCI as a reaction to the nearby positive features. The brightest part of the nebulosity corresponds to $H = 12.7$ mag arcsec^{-2}. (b) The signal-to-noise map of the same image, calculated in concentric annuli around the star. The outer wings of the nebulosity are rendered more visible. The stretch is $[-2.5\sigma, 2.5\sigma]$. (c) Interferometry image of the disk gap at 1.4 mm taken from Piétu et al. (2006). The cross represents the major and minor axes of the nebulosity. (d) The HiCIAO *H*-band image after reference PSF subtraction. The circular halo out to ∼0″6 is most likely an artifact from imperfect PSF matching. (e) The NACO K_s-band image after reference PSF subtraction, for comparison.

for this run, producing high contrast at a small inner working angle.

3. RESULTS

3.1. Imaging of the Disk Gap

The *H*-band HiCIAO images reveal a crescent-shaped nebulosity around LkCa 15 after both conservative LOCI reduction with a frame selection criterion of 3 FWHM and conventional reference PSF subtraction (Figure 1). With a diameter of ∼1″2 (≈170 AU), it is elongated along the position angle ∼60°, leaving localized traces in the concentric annuli around the star in which LOCI operates. The consistency of the LOCI and reference subtraction images demonstrates that the nebulosity is elliptical enough to survive conservative LOCI largely
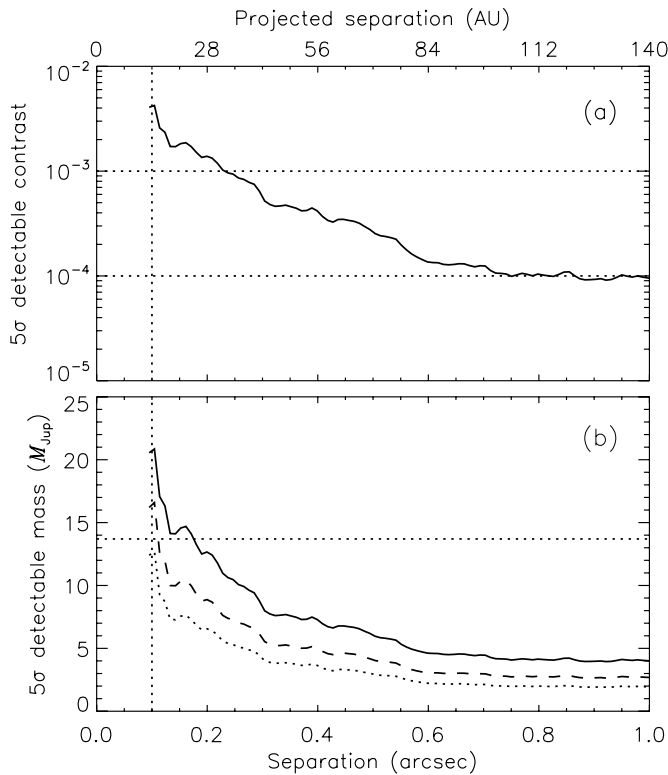
Figure 2. Contrast (a) and mass (b) of companions detectable at 5σ around LkCa 15, based on the *H*-band LOCI image after convolution with a circular aperture of 4 pixel (38 mas) in diameter. The contrast values are converted into companion mass using the COND evolutionary models by Baraffe et al. (2003) assuming a distance of 140 pc and an age of 5 Myr (solid curve), 3 Myr (dashed curve), and 1.5 Myr (dotted curve), respectively. The vertical dotted lines mark the inner working angle of ADI in this data set. The horizontal dotted lines guide the eye in (a) and indicate the deuterium burning limit of 13.7 $M_{\rm Jup}$ in (b). No companion candidates are detected.

Figure 3. Profile of the disk wall edges derived from an 11 pixel wide strip cut from the LOCI image along the perceived major axis of the ellipses in Figure 4 (position angle $-32°.8$), collapsed along the strip width and then median smoothed on the scale of 5 pixels ($\sim$1 FWHM), shown as a black curve. Median smoothing conserves edges well while removing pixel-to-pixel noise. The red vertical curve in the center is the bisector of the two opposed slopes of the profile, demonstrating the asymmetry. The orange curve shows the same smoothed profile taken from the LOCI image after rescaling with a map of the squared distance r^2 from the star. The dashed horizontal lines guide the eye.

(A color version of this figure is available in the online journal.)

intact. Although some flux is inevitably lost in this process, the elimination of the star's PSF in LOCI is superior to conventional reference PSF subtraction, revealing the sharp inner and outer edges of the structure clearly. The crescent is also found in the PSF-subtracted $K_{\rm s}$-band images from VLT/NACO, supporting the interpretation that it represents a real astronomical feature. The gap enclosed by the inner edge matches the gap predicted from the SED (Espaillat et al. 2007) as well as the localized flux deficit seen in 1.4 mm interferometry (Piétu et al. 2006, cf. Figure 1) in terms of size, ellipticity, and position angle.

The negative areas in the inner field represent oversubtraction, which is inevitable in LOCI when strong signals are present. The algorithm attempts minimize the root mean squares of the residual image, thus the positive mean offset of a signal will be lost, given that it cannot be distinguished from the positive mean offset of the stellar PSF halo. In conservative LOCI, the frame selection criterion that allows the survival of azimuthally extended positive flux concentrations also produces extended oversubtraction areas. This effect renders the flux levels in the resulting image unreliable, but preserves sharp edges in the original flux distribution. Similarly, the location of a point source in regular LOCI is reliable, but its photometry is not, requiring the determination of a correction factor.

In its brightest pixel, the crescent in the LOCI image reaches a peak intensity of $H = 12.7$ mag arcsec^{-2}, which is to be taken as a conservative lower limit. Reference PSF subtraction is expected to retain all of the disk flux, but the central part
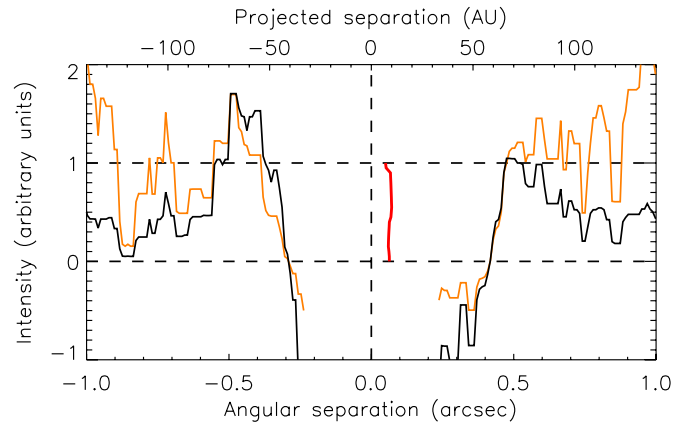
of the image is dominated by strong residuals from the PSF subtraction and therefore does not provide a better photometric measurement.

The small extended signal $0''.35$ to the southeast of the star in the *H*-band images likely corresponds to a real physical feature, given that it is visible both after LOCI processing and after reference PSF subtraction (Figures 1(a) and 1(d)).

3.2. Constraints on Point Sources

Our LOCI imaging allows us to set upper limits on the point sources present in the vicinity of LkCa 15. Figure 2 shows the companion mass that we can exclude at the 5σ level as a function of separation, assuming the COND evolutionary models by Baraffe et al. (2003), a distance of 140 pc, and an age of 3–5 Myr (Simon et al. 2000). Since LkCa 15 is part of the Taurus star-forming region, for which Watson et al. (2009) give an age of 1–2 Myr, we also plot a detectable mass curve for the age of 1.5 Myr. The image was convolved with a circular aperture 4 pixel in diameter, and the noise level is calculated as the standard deviation in concentric annuli. We compensate for the expected flux loss due to partial self-subtraction by implanting test point sources in the raw frames and measuring how they are affected by the LOCI algorithm. We note that the bright nebulosity dominates the noise level at all separations, thus the calculated upper limit is likely conservative, overestimating the true residual speckle noise level. We do not detect any statistically significant signals that could be considered companion candidates.

Bonavita et al. (2010) present a more detailed discussion of point-source constraints around LkCa 15, including alternate evolutionary model assumptions, based on the NACO $K_{\rm s}$-band data. They reach the same contrast levels as we do.

3.3. Pericenter Offset

We find a likely positional offset of the inner and outer boundaries of the nebulosity from the star along the system semi-major axis (Figures 3 and 4(a)). Furthermore, our inner

and outer fitted ellipses are rotated by $-4°$ and $-3°$ with respect to the position angle of $150°.7$ in Piétu et al. (2007), with an estimated fitting error of $2°$.

In order to quantify the observed offset, we cut a strip with a width of 11 pixels $= 0''.10$ centered on the star and oriented along the major axis of our fitted ellipses from the LOCI image, assuming a $-3°.5$ offset from the 1.4 mm position angle. Since the disk does not suffer from foreshortening along its apparent major axis, the distances along the strip are a direct measure of physical distance. We collapse the strip into a one-dimensional profile, plotted in Figure 3.

The intensity drops down to zero over a distance of 54 mas ($\approx$8 AU, 1.0 FWHM) on the west side and 81 mas ($\approx$11 AU, 1.5 FWHM) on the east side of the gap, indicating that the edge is sharp at or below the image resolution. The bisecting curve between the two opposed gap edges reveals a systematic offset from the star's position by 64 mas (9 AU) with a standard deviation of 6 mas (0.9 AU). Since the star is unsaturated, its centering accuracy ($\sim$0.2 pixels $=$ 2 mas) does not contribute significantly to the uncertainty. The distance of the gap edges from the star is 345 mas $=$ 48 AU on the left side and 447 mas $=$ 63 AU on the right side at an accuracy of 9 mas (1.3 AU), consistent with the 46 AU radius derived from millimeter interferometry by Piétu et al. (2006).

After scaling each pixel in the strip by r^2 before collapsing the strip, we find that the nebulosity appears at roughly the same brightness on both sides of the gap, suggesting an r^{-2} dependency of the unscaled flux levels. This is consistent with the assumption that we are looking at reflected light from material at varying distances r from the star.

Thus, the inner edge of the outer disk around LkCa 15 likely features a pericenter offset comparable to those observed in the disks of HD 142527 (Fukagawa et al. 2006) and Fomalhaut (Kalas et al. 2005).

4. DISCUSSION

4.1. Forward-scattering Scenario

One possible explanation of the observed bright nebulosity is forward scattering, which is commonly invoked to explain the brightness asymmetries in disk surfaces seen in reflected light (e.g., Weinberger et al. 1999; Fukagawa et al. 2006). Forward scattering on large dust grains can be several times as efficient as backward scattering; as a result, the near-side surface of such a disk appears brighter than the far side. This requires the outer disk surface to be illuminated by the star. The first of the two SED-compliant models in Mulders et al. (2010) includes a forward-scattering disk surface; furthermore, the far-side gap wall is shadowed by an optically thick inner disk, rendering it hard to detect in direct imaging (Figure 4(c)). Note that the size and shape of the dust grains in the wall are not well known. This scenario is supported by Piétu et al. (2007), whose orientation and inclination values for the LkCa 15 disk suggest that the northwest side is the near side, as well as the fact that the crescent seen after reference PSF subtraction features a bright spot along the minor axis.

4.2. Illuminated Wall Scenario

Another explanation for the nebulosity is that it represents the inner wall of the outer disk on the far side of the star, illuminated by the star and viewed directly through the disk gap (Espaillat et al. 2008; Figure 4(b)). The illuminated surface of the near-side wall, on the other hand, is blocked from sight by
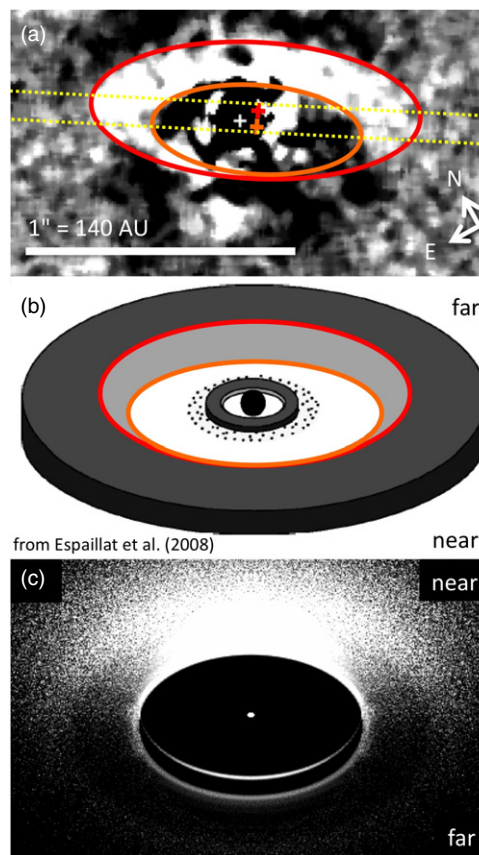

Figure 4. (a) Ellipse fits to the inner and outer boundaries of the scattered light nebulosity seen in the HiCIAO *H*-band LOCI image after median filtering on the spatial scale of 5 pixels $\approx$1 FWHM and de-rotation by $-29°.3$ (based on the position angle of $150°.7$ in Piétu et al. 2007). The inner (orange) and outer (red) ellipses are offset from the star along the major axis by 51 mas and 57 mas and rotated by $-4°$ and $-3°$, respectively. Their centers are marked by orange and red plus signs, respectively, while the star's position is indicated by a white plus sign. The dotted lines delimit the area on which the quantitative analysis in Figure 3 is based (offset angle $-3°.5$). (b) Sketch of the illuminated wall scenario, taken from Espaillat et al. (2008), based solely on the SED and millimeter interferometry. The inner disk is not to scale. The illuminated disk wall on the far side (light gray) is directly visible while the near-side wall blocks its bright side from view. (c) *H*-band image of the forward-scattering scenario including anisotropic scattering, from the simulation presented in Mulders et al. (2010). The near-side disk surface (top) appears bright due to efficient forward scattering, whereas the far-side disk wall (bottom) is mostly shadowed by the inner disk (center, not resolved), reducing the wall image to two thin parallel arcs.

(A color version of this figure is available in the online journal.)

the bulk of the optically thick disk. Furthermore, the wall is high enough to cast the outer surface of the disk into shadow, suppressing a forward-scattering signature. This corresponds to the second model by Mulders et al. (2010). The morphology of the nebulosity favors this scenario, given that (1) there is a sharp outer edge roughly parallel to the inner edge, (2) the nebulosity reaches across the major axis, "embracing" the star, and (3) the nebulosity is wider along the major axis than along the minor, all of which are expected for an illuminated tapered disk wall, but not for forward scattering on the disk surface. Thus, we consider the illuminated wall scenario the more likely explanation until further data become available.

4.3. Gap Formation Mechanism

Both scenarios presented above must invoke a disk gap to explain the sharp inner edge of the observed nebulosity. Our data

therefore prove the validity of the gapped disk model predicted from the SED.

Several mechanisms have been proposed to produce cavities or gaps in protoplanetary disks. Magneto-rotational instability (MRI) as described in Chiang & Murray-Clay (2007) can be excluded for LkCa 15, since it acts on all disk components that can be ionized by direct X-ray illumination from the star, thus the inner dust component of LkCa 15 known from the SED could not have survived. Furthermore, the stellar mass of $0.97\,M_\odot$ and stellar accretion rate of $2.4 \times 10^{-9}\,M_\odot\,\mathrm{yr}^{-1}$ (Espaillat et al. 2007) would require a viscosity parameter $\alpha \approx 0.0007$, one order of magnitude below the range considered in the publication. While photoevaporation can in principle evacuate gaps as large as that of LkCa 15 in simulations (Alexander et al. 2006; Gorti et al. 2009; Owen et al. 2010), those require that the inner disk drain away entirely before the gap can grow beyond 1–10 AU. The presence of an inner dust disk around LkCa 15 does not fit this scenario.

Espaillat et al. (2008) therefore conclude that dynamical clearing by one or more orbiting bodies is the most plausible cause of the disk gap. Our detection of a likely pericenter offset in the LkCa 15 disk gap reinforces this argument. Dynamical sculpting is commonly invoked to explain warps and eccentricities in debris disks (e.g., Roques et al. 1994; Kalas et al. 2005), and also produces off-centered gaps in simulations of protoplanetary disks (e.g., Marzari et al. 2010). In contrast, neither MRI nor photoevaporation have been predicted to cause such effects.

In the case of LkCa 15, close stellar companions are excluded by long baseline interferometry (Pott et al. 2010), while our data conservatively exclude companions more massive than $21\,M_{\mathrm{Jup}}$ exterior to $0''\!.1$ (14 AU) and all but planetary-mass bodies exterior to $0''\!.2$ (28 AU). Piétu et al. (2006) note that a 5–$10\,M_{\mathrm{Jup}}$ body orbiting at 30 AU (the equivalent of Neptune's orbit) has a sufficiently large Hill sphere to dynamically produce a wall at 50 AU. Less massive bodies orbiting closer to the wall can have similar dynamical effects. Lubow et al. (1999) note that bodies more massive than $6\,M_{\mathrm{Jup}}$ will suppress accretion onto a young solar analog to levels below that still present in the LkCa 15 system. Our data indicate that any bodies in the disk of LkCa 15 at $r \geqslant 0''\!.2$ (28 AU) from the primary in projection must have planetary masses.

We therefore find dynamical clearing by one or more planets to be the most likely cause of LkCa 15's disk gap. Given the Sun-like mass of the young star ($0.97\,M_\odot$), we might in fact be looking at a solar system analog in the making.

REFERENCES

Alexander, R. D., Clarke, C. J., & Pringle, J. E. 2006, MNRAS, 369, 229
Baraffe, I., Chabrier, G., Barman, T. S., Allard, F., & Hauschildt, P. H. 2003, A&A, 402, 701
Bonavita, M., et al. 2010, arXiv:1004.3487
Brown, J. M., Blake, G. A., Qi, C., Dullemond, C. P., Wilner, D. J., & Williams, J. P. 2009, ApJ, 704, 496
Bryden, G., Chen, X., Lin, D. N. C., Nelson, R. P., & Papaloizou, J. C. B. 1999, ApJ, 514, 344
Calvet, N., D'Alessio, P., Hartmann, L., Wilner, D., Walsh, A., & Sitko, M. 2002, ApJ, 568, 1008
Chiang, E., & Murray-Clay, R. 2007, Nature Phys., 3, 604
Espaillat, C., Calvet, N., D'Alessio, P., Hernández, J., Qi, C., Hartmann, L., Furlan, E., & Watson, D. M. 2007, ApJ, 670, L135
Espaillat, C., Calvet, N., Luhman, K. L., Muzerolle, J., & D'Alessio, P. 2008, ApJ, 682, L125
Fukagawa, M., Tamura, M., Itoh, Y., Kudo, T., Imaeda, Y., Oasa, Y., Hayashi, S. S., & Hayashi, M. 2006, ApJ, 636, L153
Gorti, U., Dullemond, C. P., & Hollenbach, D. 2009, ApJ, 705, 1237
Henning, Th., et al. 2010, ApJ, 714, 1511
Hodapp, K. W., et al. 2008, Proc. SPIE, 7014, 42
Kalas, P., Graham, J. R., & Clampin, M. 2005, Nature, 435, 1067
Lafrenière, D., Marois, C., Doyon, R., Nadeau, D., & Artigau, É. 2007, ApJ, 660, 770
Lubow, S. H., Seibert, M., & Artymowicz, P. 1999, ApJ, 526, 1001
Marois, C., Lafrenière, D., Doyon, R., Macintosh, B., & Nadeau, D. 2006, ApJ, 641, 556
Marois, C., Macintosh, B., Barman, T., Zuckerman, B., Song, I., Patience, J., Lafrenière, D., & Doyon, R. 2008, Science, 322, 1348
Marzari, F., Baruteau, C., & Scholl, H. 2010, A&A, 514, L4
Mulders, G. D., Dominik, C., & Min, M. 2010, A&A, 512, A11
Owen, J. E., Ercolano, B., Clarke, C. J., & Alexander, R. D. 2010, MNRAS, 401, 1415
Piétu, V., Dutrey, A., & Guilloteau, S. 2007, A&A, 467, 163
Piétu, V., Dutrey, A., Guilloteau, S., & Chapillon, E. 2006, A&A, 460, L43
Pott, J.-U., Perrin, M. D., Furlan, E., Ghez, A. M., Herbst, T. M., & Metchev, S. 2010, ApJ, 710, 265
Ratzka, T., Leinert, C., Henning, T., Bouwman, J., Dullemond, C. P., & Jaffe, W. 2007, A&A, 471, 173
Roques, F., Scholl, H., Sicardy, B., & Smith, B. A. 1994, Icarus, 108, 37
Sargent, B. A., et al. 2009, ApJS, 182, 477
Simon, M., Dutrey, A., & Guilloteau, S. 2000, ApJ, 545, 1034
Tamura, M. 2009, in AIP Conf. Ser., 1158, Exoplanets and Disks: Their Formation and Diversity, ed. T. Usuda, M. Tamura, & M. Ishii (Melville, NY: AIP), 11
Thalmann, C., et al. 2009, ApJ, 707, L123
Watson, D. M., et al. 2009, ApJS, 180, 84
Weinberger, A. J., Becklin, E. E., Schneider, G., Smith, B. A., Lowrance, P. J., Silverstone, M. D., Zuckerman, B., & Terrile, R. J. 1999, ApJ, 525, L53